



Analysis and characterization of surface oxides on intermetallic alloys of zirconium using auger electron spectroscopy
by Rajesh G Mirpuri

A thesis submitted in partial fulfillment of the requirements for the degree of Master of Science in Chemical Engineering
Montana State University
© Copyright by Rajesh G Mirpuri (1991)

Abstract:

The surface composition of oxidized zirconium and nickel and their oxidized intermetallics, $ZrNi_3$, $ZrNi$, $ZrNi_5$ and Zr_2Ni_7 are evaluated. This was performed following the installation and set-up of an Auger electron spectroscope and development of relevant software for both digital process control and data analysis.

Surface oxide layers formed on the samples under two different conditions, room temperature and at $300^\circ C$ for 1 hour were analyzed. Depth profiles were performed using Auger electron spectroscopy and argon ion sputtering. The zirconium and nickel concentrations increased and the oxygen concentration decreased with increase in sputtering time. Longer sputter times were noticed in the case of the samples oxidized at $300^\circ C$ indicating thicker oxide layers. The oxide layer formed at $300^\circ C$ on zirconium was thicker than the oxide layer on nickel at $300^\circ C$ since the former required 90 minutes of sputtering compared to 4 minutes of sputtering for the latter. The oxide layer formed on zirconium at $300^\circ C$ is shown to have a ZrO_2 stoichiometry.

The sputter depth profiles on the intermetallics are consistent with earlier work reported in the literature, with a slight discrepancy in the steady state final intensities of the zirconium and nickel peaks noticed in the case of the intermetallics oxidized at $300^\circ C$. This can be attributed to a change in the primary Auger electron beam energy from 3 keV to 2 keV which diminished the peak intensities significantly. Surface cracks on the intermetallic surfaces which are laterally oxidized during high temperature oxygen exposure may have also resulted in the attenuation of the nickel and zirconium peak intensities and the increase in oxygen peak intensity.

ANALYSIS AND CHARACTERIZATION OF SURFACE OXIDES ON
INTERMETALLIC ALLOYS OF ZIRCONIUM USING
AUGER ELECTRON SPECTROSCOPY

by

Rajesh G. Mirpuri

A thesis submitted in partial fulfillment
of the requirements for the degree

of

Master of Science

in

Chemical Engineering

MONTANA STATE UNIVERSITY
Bozeman, Montana

May 1991

N378
M6792

APPROVAL

of a thesis submitted by

Rajesh G. Mirpuri

This thesis has been read by each member of the thesis committee and has been found to be satisfactory regarding content, English usage, format, citations, bibliographic style, and consistency, and is ready for submission to the College of Graduate Studies.

June 11, 1991
Date

Max C. Deibert
Chairperson, Graduate Committee

Approved for the Major Department

June 11, 1991
Date

John T. Sears
Head, Major Department

Approved for the College of Graduate Studies

August 6, 1991
Date

Henry L. Parsons
Graduate Dean

STATEMENT OF PERMISSION TO USE

In presenting this thesis in partial fulfillment of the requirements for a master's degree at Montana State University, I agree that the Library shall make it available to borrowers under rules of the Library. Brief quotations from this thesis are allowable without special permission, provided that accurate acknowledgement of source is made.

Permission for extensive quotation from or reproduction of this thesis may be granted by my major professor, or in his/her absence, by the Dean of Libraries when, in the opinion of either, the proposed use of the material is for scholarly purposes. Any copying or use of the material in this thesis for financial gain shall not be allowed without my written permission.

Signature Rajesh G. Mishra

Date June 11th 1991

TABLE OF CONTENTS

	Page
APPROVAL	ii
STATEMENT OF PERMISSION TO USE	iii
TABLE OF CONTENTS	iv
LIST OF TABLES	vi
LIST OF FIGURES	vii
ABSTRACT	ix
1. INTRODUCTION	1
2. BACKGROUND	6
Research Objectives	10
3. OXIDATION OF METALS AND ALLOYS	11
Low Temperature Oxidation	12
Diffusion in Oxides	13
Lattice Defects	14
Lattice Diffusion	14
Diffusion Mechanisms	16
High Temperature Oxidation of Metals	17
Compact Oxide Scales	17
Porous Oxide Scales	21
High Temperature Oxidation of Metals & Alloys	22
4. EXPERIMENTAL METHOD	26
Auger Electron Spectroscopy	26
Experimental System	29
Ultra-High Vacuum Systems	29
Ion Gun	30
Sample Mount System	32
Energy Analyzer	36
Sample Preparation	38
Surface Preparation	39
Sample Alignment	40
Elastic Peak Procedure	41
Acquiring AES Data	41
Shut Down Procedure	41
5. RESULTS	42
6. INTERPRETATION	68

TABLE OF CONTENTS-CONTINUED

	Page
7. SUMMARY AND CONCLUSIONS	80
8. RECOMMENDATIONS FOR FURTHER RESEARCH	82
REFERENCES	84

LIST OF TABLES

Table	Page
1. Steady State Intensity Profile Data of Zr1 peak for the metal and intermetallic samples analyzed	71
2. Steady State Intensity Profile of Ni1 and Ni2 peaks for the metal and intermetallic samples analyzed	73
3. The sputter time required to remove the oxide layer for the metal and intermetallic samples	78

LIST OF FIGURES

Figure	Page
1. Wagner Schematics for Oxidation of Alloys	19
2. Wagner Schematics for Oxidation of Metal Alloys	25
3. Energetics of the Auger process	27
4. AES Analytical Equipment	31
5. Sample Holder for AES Analysis	33
6. Relative Orientation of Sample Mount with Ion Gun and Electron Gun	35
7. The Electron Gun and CMA Arrangement	37
8. AES Survey of Zirconium Foil	43
9. AES Survey of Sputter Cleaned Zirconium	44
10. Expanded energy region of Sputter Cleaned Zirconium	45
11. Multiplexed Zr ₂ Peak on Zirconium Foil	47
12. Multiplexed Zr ₂ Peak on Sputter Cleaned Zirconium ...	48
13. Multiplexed Zr ₁ Peak on Sputter Cleaned Zirconium ...	49
14. Multiplexed Oxygen Peak on Zirconium	51
15. Sputter Depth Profile for Zr	52
16. Sputter Depth Profile for Zr(ox)	53
17. AES Survey of Nickel Foil	54
18. AES Survey of Sputter Cleaned Nickel	56
19. Multiplexed Ni ₁ Peak on Sputter Cleaned Nickel	57
20. Multiplexed Ni ₂ Peak on Sputter Cleaned Nickel	58
21. Sputter Depth Profile for Ni	59
22. Sputter Depth Profile for Ni(ox)	60

LIST OF FIGURES - CONTINUED

Figure	Page
23. Sputter Depth Profile for ZrNi ₅	61
24. Sputter Depth Profile for Zr ₂ Ni ₇	63
25. Sputter Depth Profile for ZrNi ₃	64
26. Sputter Depth Profile for ZrNi	65
27. Sputter Depth Profile for ZrNi ₅ (ox)	66
28. Sputter Depth Profile for ZrNi ₃ (ox)	67
29. Steady State Intensity Profile for Zr	72
30. Steady State Intensity Profile for Ni	74
31. An Optical Microscope Photograph of Polished ZrNi ₃ after Oxidation at 300°C	76

ABSTRACT

The surface composition of oxidized zirconium and nickel and their oxidized intermetallics, $ZrNi_3$, $ZrNi$, $ZrNi_5$ and Zr_2Ni_7 are evaluated. This was performed following the installation and set-up of an Auger electron spectroscope and development of relevant software for both digital process control and data analysis.

Surface oxide layers formed on the samples under two different conditions, room temperature and at $300^\circ C$ for 1 hour were analyzed. Depth profiles were performed using Auger electron spectroscopy and argon ion sputtering. The zirconium and nickel concentrations increased and the oxygen concentration decreased with increase in sputtering time. Longer sputter times were noticed in the case of the samples oxidized at $300^\circ C$ indicating thicker oxide layers. The oxide layer formed at $300^\circ C$ on zirconium was thicker than the oxide layer on nickel at $300^\circ C$ since the former required 90 minutes of sputtering compared to 4 minutes of sputtering for the latter. The oxide layer formed on zirconium at $300^\circ C$ is shown to have a ZrO_2 stoichiometry.

The sputter depth profiles on the intermetallics are consistent with earlier work reported in the literature, with a slight discrepancy in the steady state final intensities of the zirconium and nickel peaks noticed in the case of the intermetallics oxidized at $300^\circ C$. This can be attributed to a change in the primary Auger electron beam energy from 3 keV to 2 keV which diminished the peak intensities significantly. Surface cracks on the intermetallic surfaces which are laterally oxidized during high temperature oxygen exposure may have also resulted in the attenuation of the nickel and zirconium peak intensities and the increase in oxygen peak intensity.

CHAPTER 1

INTRODUCTION

The development of metal alloys which have improved resistance to surface oxidation, has a major impact on the cost, durability and utility of equipment and components utilized in high temperature and other corrosive environments. The useful life of metallic components incorporated into structures and electrical systems operated under ambient conditions can also be significantly extended through appropriate alloying to improve their resistance to oxidation. Thus a more fundamental in-depth knowledge of improved metal alloys and composites, which demonstrate enhanced corrosion resistance and high temperature stability, would greatly benefit modern industry.

The reaction of oxygen with metal alloy surfaces is such that it can lead to the formation of a cohesive surface oxide layer, which protects the alloy from further significant oxidation. An in-depth study on this reaction would help in the development of metal alloys especially suited to a large range of future and current applications requiring oxidation resistance. Extensive literature[1,2,3] on the methods of relating surface oxidation mechanisms and oxide structures of pure metals provides the basis for the design and conduct of this investigation on the surface oxidation of metal alloys.

By enhancing the protective surface oxide layer, which can be either porous or compact, improved oxidation resistance is usually realized in metals and alloys. Compact oxide layers offer the best protection against high temperature oxidation because they form a nonporous barrier between the unreacted metal and oxidizing environment. Thus oxidation resistance in alloys in which at least one of the components combine readily with oxygen can be generally attributed to surface layers which are effective barriers to further oxidation of the bulk[4]. On oxidation of a metal alloy, where the base metal oxidizes rather rapidly, the base metal oxide forms on the outer scale and the oxide of the alloying element forms on the inner scale[2,3]. The ratio of the components in a surface oxide layer can be different from that in the bulk. The surface oxide thickness keeps increasing until it inhibits further growth. Cracking or flaking of these oxidized layers leads to the loss of their protective property. If the oxide layer cracks, then the metal alloy can return to its initial stage and the oxidation rate increases. On the contrary, if the resulting oxide layer remains intact and is cohesive, it will eventually resist, by virtue of reduced oxygen permeability, any further significant growth in the oxide layer thickness.

The Wagner oxidation model for metal alloys[2,3] indicates that the growth rate of a compact surface oxide layer decreases with time and increasing oxide layer

thickness. When a clean metal alloy is exposed to an oxidizing atmosphere, initial reaction kinetics controls the extent of oxide formation of each of the metallic components. Once a oxide layer forms on the surface of the alloy, further oxidation is limited by the diffusion of the oxygen through the oxide layer. Concentration gradients develop in the metal near the metal/oxide interface. The rate of oxygen diffusion into the alloy will depend in part on the concentrations of the metal oxides resulting from the surface oxidation reaction and partly on the diffusivities of oxygen in both the developing oxide layer and the metallic elements in the underlying reduced alloy.

The surface oxidation characteristics of the intermetallic alloys of zirconium make an excellent choice as a subject for investigation because of zirconium's industrial importance and the fact that it has received little previous attention in this area. Zirconium is used extensively[5] in the nuclear power industry as a major constituent of various fuel cladding alloys that separate the fuel from coolant water in atomic reactors. The most widely used alloys, zircalloys, as they are commonly known, consist of zirconium, together with tin, chromium, iron, nickel etc. which are added to promote better corrosion resistance. An important property of zirconium is its low capture cross section for neutrons i.e., neutrons pass freely through the internal zirconium structure without an appreciable energy loss and a corresponding

temperature rise in the cladding material[6]. Zirconium based fuel cladding alloys are resistant to the corrosive environment inside the atomic reactors.

The corrosive resistance of zirconium based alloys is due to the formation of thin, protective, cohesive surface oxide layers. Extensive work[6] has been carried out on the kinetics of bulk oxidation of zirconium and its alloys at elevated temperatures under different environments including air, water, steam and oxygen.

The primary method of analyzing the composition of oxide surface layers in this study is Auger Electron Spectroscopy (AES) which lends itself to investigating the atomic composition of the surface strata of clean and oxidized alloys[7]. One of the most interesting applications of quantitative AES analysis is the depth profiling technique, in which surface atoms are removed by ion bombardment with AES[8] analysis of surface composition at sequential depths. The equipment used in AES depth profiling is equivalent to a standard Auger spectrometer in combination with an ion gun. The ion gun is used to bombard the surface atoms of the sample at a relatively slow rate, and remove surface atoms almost atomic layer by layer. If a quantitative AES analysis is carried out during ion bombardment, the results yield the composition of the sample at different depths.

Single phase metals are a better choice for a surface study of the present type even though most important alloys

consist primarily of polyphase composites of solid solutions and intermetallic compounds(IC's). The main drawback in using polyphase alloys is that spectroscopic information gathered after the oxidation of these alloys is difficult to interpret due to the probable presence of more than one surface phase[1]. This complication can be circumvented by utilizing alloy compositions corresponding to intermetallic compounds which are multi-element single phase metals. The information thus developed can then be used to model the oxidation resistance of composite alloys from an improved understanding of the surface oxidation properties of their individual solid phases.

CHAPTER 2

BACKGROUND

Techniques of Electron Spectroscopy, especially, Auger Electron Spectroscopy, have been employed to study the interaction of oxygen with various metal surfaces. The types of metallic surfaces analyzed include pure metals and intermetallic compounds in both single crystal and polycrystalline form and composite alloys of intermetallics and solid solutions. These materials have been subjected to wide ranges of temperatures, pressures and durations of exposures to various oxidizing atmospheres. Several surface analytical methods have been used in combination with argon ion milling for depth profiles. The most extensively used methods are the Secondary Ion Mass Spectroscopy (SIMS) and the Electron Spectroscopy methods, in particular Auger Electron Spectroscopy (AES) and X-ray Photoelectron Spectroscopy (XPS).

The oxidation behavior of both single and polycrystalline samples of zirconium have been investigated. It has been shown that a cohesive surface oxide layer, which has a ZrO_2 stoichiometry is formed on bulk zirconium [4]. The initial exposure of zirconium to oxygen results in the formation of a nuclei of surface oxide which grow to coalescence and completion at an O_2 exposure of 30 to 60 L (1 L = 10^{-6} Torr.s) and has a thickness of approximately 2 nm at room temperature.

Since this oxidation proceeds slowly there is a transition region of intermediate oxides between the ZrO_2 layer and the bulk Zr [1].

The formation of the thin ZrO_2 surface layer on Zr protects the underlying metal from further significant oxidation at 300 K, since the diffusion of O_2 through ZrO_2 is very slow. However at higher temperatures, oxygen permeation into the bulk metal from the surface oxide layer occurs at measurable rates due to increased oxygen diffusivity and solubility in Zr.

J.S. Foord et al., studied the adsorption of D_2 , CO, N_2 , NO and O_2 on Zr at 300 K [9]. Work function, electron impact, Auger, and diffusion data indicated that heating of these adsorbed phases leads to rapid surface to bulk oxygen diffusion and very little desorption.

A related study [10] conducted by P.Sen et al., investigated the surface oxidation of three metglasses in the copper-zirconium system by employing X-ray Photoelectron Spectroscopy and Auger Electron Spectroscopy to compare their oxidation behavior with that of the corresponding crystalline states of the alloys. The study was conducted over a wide range of oxidation temperatures, pressures and alloy compositions. It was shown that both glassy and crystalline states of the Cu-Zr alloys exhibit preferential oxidation at intermediate oxygen exposures.

The surface oxidation of pure zirconium and its dilute binary alloys with tin, chromium and iron has been investigated by XPS. In this study Lalit Kumar et al., compared the oxidation behavior of zirconium and its alloys at room temperature [11]. It was observed that mostly suboxides of Zr are formed during the initial stages of oxidation at oxygen exposures less than 10 L, while at higher exposures, ZrO_2 is the dominant oxide species formed, although two suboxides are present. Pure Zr as well as its dilute alloys exhibit a decreasing rate of oxidation with increasing oxygen exposure.

Bertolini et al., analyzed the surface metallic properties of $Ni_{63.7}Zr_{36.2}$ alloy by Auger electron spectroscopy and photoelectron spectroscopy in combination with argon ion bombardment [12]. The elemental composition as a function of depth below the surface was analyzed. A thin ZrO_2 oxide layer was observed to extend up to 15-35 Å below the outer surface beyond which an abrupt interface with the $Ni_{63.7}Zr_{36.2}$ alloy existed.

Several studies of the surface oxidation behavior of nickel-zirconium intermetallic compounds have been conducted. Wright, Cocke and Owens conducted a detailed study [13] on five Ni-Zr intermetallic compounds, Zr_2Ni , $ZrNi$, $ZrNi_3$, Zr_2Ni_7 and $ZrNi_5$. The analysis included sputter cleaning of the metal alloys by argon ion milling followed by exposure to sequential treatments of hydrogen, oxygen, and hydrogen a second time.

These experiments were carried out at room temperatures and at 400°C. The depth concentration profiles were then analyzed using high resolution AES. The results showed that the surface was covered by ZrO₂ after exposure to air at room temperature and covered by NiO after high temperature oxidation at 400°C. The ratio at the surface of Ni to Zr was always greater after oxidation than after reduction. This indicates a preferential oxidation of Zr over Ni when both are present in a reduced form and the outward diffusion of Ni cations through the oxide strata at 400°C during oxidation.

Deibert and Wright investigated [14] two of the above mentioned intermetallics, ZrNi₃ and Zr₂Ni₇, by high resolution Auger Spectroscopy and Ar ion sputtering. The intermetallics were subjected to sequential hydrogen, oxygen and hydrogen treatments. The results indicate an essentially pure reduced Ni surface on a layer of oxidized zirconium, which in turn is supported on the unaltered alloy. The reduced nickel constituted a highly active catalyst surface for various reactions of possible industrial relevance. The thickness of the reduced Ni layer is estimated to be between 10 and 20 nm.

In another series of experiments by Deibert and Wright [15], the initial surface oxidation of sputter cleaned nickel-zirconium intermetallics (ZrNi₅, Zr₂Ni₇, ZrNi₃, ZrNi, ZrNi₃) at room temperature was investigated by quantitative Auger analysis and argon ion sputtering. The sputter-cleaned surfaces of the alloys were shown to be enriched in Zr

relative to their bulk, especially for the alloys which are relatively dilute in Zr. The experimental results indicate that the ratio of the sputtering rate of Ni to that of Zr is dependent on the composition of the alloy.

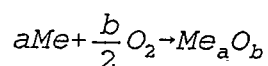
Research Objectives

- * Installation and set-up of the PHI Auger Electron Spectroscopy and development of relevant software for both digital process control and data analysis.
- * Study of the surface compositions of the oxidized intermetallic compounds of zirconium and nickel including $ZrNi_3$, $ZrNi$, $ZrNi_5$ and Zr_2Ni_7 and oxidized zirconium and nickel metal foils.
- * Develop an improved understanding of the surface oxidation of the zirconium alloys at 300°C.
- * Compare the results of this study with recent studies of Zr-Ni intermetallics, with particular emphasis on oxidation of the intermetallics.

CHAPTER 3

OXIDATION OF METALS AND ALLOYS

The total chemical equation for the reaction between a metal and oxygen gas is:



Though this appears to be a simple equation, the reaction path and the oxidation behavior of a metal depends on a variety of factors. The metal oxidation reaction mechanisms, as a result, are complex.

The initial step in the metal-oxygen reaction involves the adsorption of gas on the metal surface. As the reaction proceeds, oxygen may dissolve in the metal; then oxide is formed on the surface as an oxide layer. Both the adsorption and the initial oxide formation are functions of surface orientation, crystal defects at the surface, surface preparation, and impurities in both the metal and the gas [16].

The surface oxide separates the metal and the gas. When a compact film covers the surface, the reaction proceeds through a solid-state diffusion of the reactants through the film. For thin films the driving force for this transport of reactants is mainly due to electric fields (migration of charged imperfections) in or across the film. For thick films

or scales it is determined by the chemical potential gradient across the scale [17].

Metals may also form porous oxide scales which as such do not serve as a solid-state diffusion barrier between the reactants. In such cases the reaction may be limited by processes occurring at phase boundaries. At high temperatures, oxides may also be liquid or volatile.

The overall driving force of metal-oxygen reactions is the free energy change associated with the formation of the oxide from the reactants. Thermodynamically the oxide will be formed only if the ambient oxygen pressure is larger than the dissociation pressure of the oxide in equilibrium with its metal [16].

Low-Temperature Oxidation

The initial step in the reaction between a metal and oxygen is the adsorption of gas on the metal surface. Then isolated oxide nuclei form at random positions on the surface. After formation of the random oxide nuclei the oxidation proceeds through a growth of the individual crystallites until the whole surface is covered with oxide. The rate of reaction during the initial stage increases with time; that is, the sticking coefficients of oxygen increases as oxygen is consumed. This increased activity is due to an initial oxide nucleation at preferred sites and the reaction proceeds through a lateral surface growth of the nuclei [16].

Dislocations, surface defects, impurities, etc., serve as nucleation sites. The adsorbed oxygen diffuses on the surface to the growing nuclei, causing an oxygen depletion in a zone around each nucleus in which no other nuclei form. The size of these zones is governed by the supply of adsorbed oxygen and the rate of surface migration [18].

Diffusion in Oxides

When a dense, compact oxide film or scale has been formed on a metal surface, the oxide separates the reactants. Thus, reaction can only proceed through a solid-state diffusion of reactants through the oxide [19]. Diffusion in solids takes place because of the occurrence of imperfections or defects in solids [16].

Imperfections in solids can be broadly divided into point or lattice defects. Vacancies, interstitial atoms, and misplaced atoms come under point defects. Line and surface defects include dislocations, grain boundaries and inner and outer surfaces. Point or lattice defects are responsible for lattice diffusion, also called volume or bulk diffusion [16].

In polycrystalline materials the relative contributions of the different types of diffusion are a function of temperature, partial pressure of the components, grain size, porosity, etc. Grain boundary diffusion has a smaller activation energy than volume diffusion and as a result becomes increasingly important at lower temperatures [20].

Lattice Defects

In a perfect crystal both the entropy and internal energy of the system increases with the creation of point defects. The equilibrium concentration of the defects will be reached when the free energy of the system is at a minimum. In any given crystal all types of defects, in principle, will be formed although the free energies of formation of different types and systems of defects will have widely different values. Correspondingly one type of defect structure commonly predominates in a particular solid at equilibrium. The relative concentrations of the different types of defects is a function of temperature and other variables which influence the state and the composition of the compound. Thus, defect equilibria with a large positive enthalpy of formation which are not favored at low temperatures, may become important at high temperatures. Lattice defects may be neutral or charged.

Lattice Diffusion

Lattice diffusion takes place through the movement of point defects. The presence of different types of defects gives rise to different mechanisms of diffusion. Fick's laws of diffusion give the mathematical relationship between the concentration gradient and the diffusion coefficient [18]. The rate of diffusion is expressed in terms of the diffusion coefficient D , which is defined by Fick's first law,

$$J = -D \left(\frac{\partial c}{\partial x} \right)_t$$

where J is the instantaneous flow rate per unit area of the diffusing species across a plane, c is the concentration of the diffusing species at the plane, and $\partial c / \partial x$ is the concentration gradient normal to the plane. Thus, the diffusion constant D is the flow rate/unit area at unit concentration gradient normal to the plane.

Fick's second law relates the concentration gradient to the change in concentration with time. For the case in which the diffusion coefficient is independent of concentration:

$$\frac{\partial c}{\partial t} = D \frac{\partial^2 c}{\partial x^2}$$

These equations can be solved under certain boundary conditions which may be closely approximated experimentally. For homogenous diffusion in a solid the concentration of the diffusing species normal to the plane is given by:

$$c = \frac{c_0}{2\sqrt{\pi Dt}} \exp\left(-\frac{x^2}{4Dt}\right)$$

where c represents the concentration at a distance x from the surface, c_0 is the concentration of the species originally present on the surface, and t the time of diffusion anneal. The typical experiment used to establish the constants in this relationship involves deposition of a very thin film of radioactive isotopes on a plane surface of a sample and, after subsequent diffusion anneal, determination of the

concentration of diffusing species as a function of distance from the plane surface [16]. If diffusion is nonhomogenous, different relationships between concentration and penetration distance may result.

The temperature dependence of the diffusion coefficient is given by:

$$D = D_0 \exp\left(-\frac{Q}{RT}\right)$$

where Q is the activation energy, and the pre-exponential factor D_0 , the frequency factor [20].

Diffusion Mechanisms

Diffusion is said to take place by a vacancy mechanism if an atom on a normal lattice site jumps into an adjacent unoccupied lattice site. If an atom moves from an interstitial site to one of its neighboring interstitial sites, the diffusion occurs by an interstitial mechanism. Such a movement, or jump, of the atom involves a considerable distortion of the lattice, and this mechanism is probable only when the interstitial atom is smaller than the atoms on the normal lattice position [20]. If the distortion during the jump becomes too large to make the interstitial mechanism probable, an interstitial atom pushes one of its nearest neighbors on normal lattice site into another interstitial position and itself occupies the lattice site of the displaced atom.

A variant of the interstitialcy mechanism is the crowdion[20]. In this case an extra atom is crowded into a line of atoms and thereby displaces several atoms along the line from their equilibrium positions.

High Temperature Oxidation of Metals

High-temperature oxidation usually results in the formation of an oxide film. The mechanism of oxidation depends on the nature of the scale, that is, whether the oxide is solid or liquid or if it also partially evaporates. If solid scales are formed, the oxidation behavior also depends on whether the scales are compact or porous.

Compact Oxide Scales

A compact scale acts as a barrier separating the metal and the oxygen gas. The rate of oxidation at high temperatures is limited by diffusion through the compact scale, provided there is sufficient oxygen available at the oxide surface. The oxide grows in thickness leading to an increase in diffusion distance. This results in a decrease in the rate of reaction with time. Compact scales offer the best protective properties. Improving the protective properties of the oxide scale leads directly to an improvement in the oxidation resistance of metals and alloys [16].

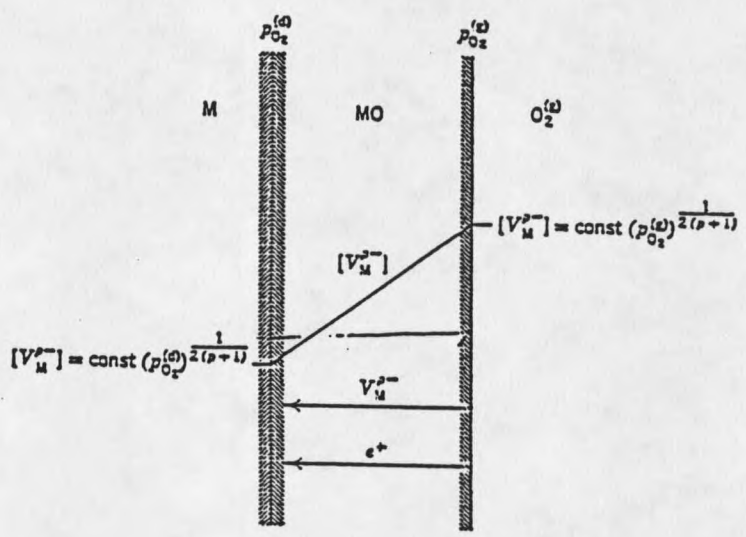
Wagner [2,3] has provided a fundamental understanding of the essential features of high temperature oxidation of pure metals in his theory of high temperature parabolic oxidation.

Figure 1 shows the Wagner schematics of concentration gradient of oxygen and metal ion vacancies and the transport processes occurring in an oxide scale containing such vacancies. The legend for Figure 1 is as follows:

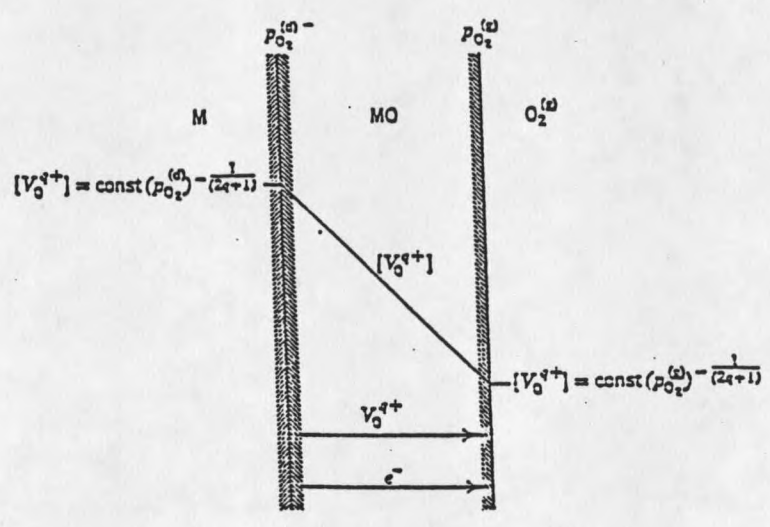
V_M^{p-}	represents metal ion vacancies
V_O^{q+}	represents oxygen ion vacancies
e^{\ddagger}	represents electron holes
e^-	represents electrons
M	represents metal
M_qO_p	represents the hypothetical metal oxide
p	represents the functional dependence of V_M^{p-} on $p_0^{(d)}$
g	represents the functional dependence of V_O^{q+} on $p_0^{(g)}$
$p_0^{(d)}$	represents dissociation pressure of oxide
$p_{O_2}^{(g)}$	represents ambient oxygen partial pressure

Wagner's theory applies to compact scales of reaction products. Volume diffusion of the reacting ions (or corresponding point defects) or a transport of electrons across the growing scale is assumed to be the rate-determining process of the total reaction. Electrons and ions are considered to migrate independently of each other. Since diffusion through the scale is rate-determining, reactions at phase boundaries are considered rapid, and it is assumed that thermodynamic equilibrium is established between the oxide and the oxygen gas at the MO/O_2 interface and between the metal and the oxide at the M/MO phase boundary [16].

The driving force of the reaction is the free-energy change associated with the formation of the oxide MO from the metal M and the oxygen gas. The partial pressure of oxygen at the M/MO interface is equal to the equilibrium dissociation



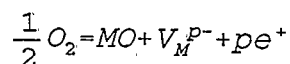
Metal Ion Vacancies



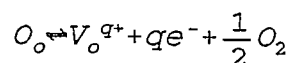
Oxygen Ion Vacancies

Figure 1. Wagner Schematics for Oxidation of Alloys

pressure of the oxide in contact with its metal, $p_{O_2}^{(d)}$, while at the oxide/oxygen interface it is equal to the oxygen pressure in the gas phase, $p_{O_2}^{(g)}$. For an oxide scale with metal ion vacancies, the metal ions diffuse outward from the M/MO to the M/MO₂ interface. The vacancies migrate in the opposite direction, and their equilibrium concentrations at the gas phase interface are given by the defect equilibrium:



When $p_{O_2}^{(g)} > p_{O_2}^{(d)}$, the metal ion vacancies are continuously produced at the MO/O₂ interface and consumed at the M/MO interface. Oxygen ion vacancies migrate in the direction opposite to the metal ion vacancies, and their equilibrium concentration at the M/MO and MO/O₂ interfaces is given by:



Oxygen ion vacancies are correspondingly created continuously at the M/MO interface and consumed at the MO/O₂ phase boundary.

The rate of growth is, in these terms, determined by the gradients and the rate of diffusion of the components. These mechanisms lead to parabolic oxidation behavior.

The Wagner theory permits an evaluation of the rate constant of high-temperature parabolic oxidation provided the diffusion coefficient is known. In evaluating experimental results the parabolic rate constant is expressed as

$$\frac{dx}{dt} = \frac{k_p}{x}$$

Here k_p is the parabolic rate constant and x , the oxide thickness. On rearranging and integrating,

$$x \propto t^{\frac{1}{2}}$$

Porous Oxide Scales

During compact oxide scale formation the rate of reaction is governed by the solid-state diffusion of the reactants through the scale, as long as sufficient oxygen is available at the oxide surface. Deviations from ideal behavior, i.e. compact and pore-free oxides, occur when porous scales form.

If the transport occurs by an outward migration of metal ions by the vacancy mechanism, vacancies may collect to form cavities and pores at the metal/oxide interface and produce appreciable porosity in the oxide scale after extended reaction. The cavities then act as barriers to the solid-state diffusion process. These oxide scales can rupture and breakup becoming non-barriers to gaseous oxygen. Also when phase boundary processes become rate-determining instead of solid-state diffusion through the scale, then porous scales may be formed. When porous scales are formed, the kinetics of the reaction is commonly found to be linear with time. The rate of initial oxidation is often observed to decrease with time indicating the formation of a protective phase before the oxidation transforms to a linear rate. Phase boundary process

limitations occur when the linear oxidation for porous scales is faster than the protective oxidation rate. Cracks can form which rupture leading to the formation of porous scales.

Thus porous scales are non-protective. These scales usually occur during later stages of the reaction because of rupture and fragmentation of the oxide scale after it has reached a critical thickness [16].

High Temperature Oxidation of Metal Alloys

Oxidation mechanisms for alloys are more complex than for pure metals. The alloyed metal atoms do not diffuse at the same rates either in the oxide or alloy phase and the components of alloys have different affinities for oxygen. As a result, oxide scales on alloys do not contain the same relative amounts of the alloy constituents as does the metallic phase. As the oxidation proceeds, the composition and structure of oxide scales often change. Thus the oxidation kinetics often markedly deviate from ideal and simple rate equations. Also, if oxygen dissolves in the alloy phase, the least noble alloy component can form oxide inside the alloy.

Since more than one oxide is formed, Wagner classified alloy oxidation in terms of different types of behavior.

1. Selective oxidation in which the least noble constituent is selectively or preferentially oxidized.
2. Formation of composite scales.
3. Formation of scales with complex oxides.

Under any set of conditions selective oxidation takes place only above a critical concentration of the active alloy component. Wagner [2,3] analyzed the conditions necessary for oxidation in binary alloys and derived a mathematical expression for this critical concentration. This can be extended to the case of composite scales and scales with complex oxides.

Wagner considered an alloy A-B in which B is the less noble metal and A and B do not react to form a double oxide or spinel. Making the assumption that compact oxides are formed, three main cases for the oxidation of the alloy A-B may be considered.

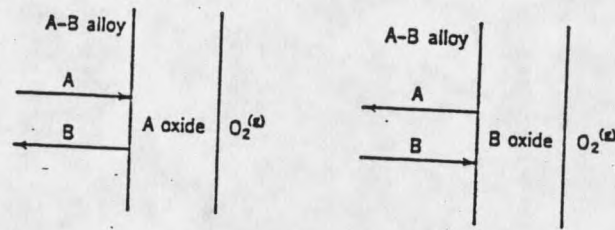
1. At low concentrations of B, only the A oxide will be formed and B will diffuse into the alloy from the alloy/oxide interface.
2. For sufficiently high concentrations of B in the alloy only the B oxide will be formed and A will diffuse into the alloy from the alloy/oxide interface.
3. At B concentrations ranging from the low concentrations in case 1 to the high concentration in case 2, A oxide and the B oxide will simultaneously be formed (composite scale).

Figure 2 shows the schematics for the three different oxidation cases. Assuming the formation of a compact, pore-free oxide scale, Wagner showed that the critical concentration N_B (above which only the B oxide is formed) is given by :

$$N_B = \frac{V}{z_B M_O} \left(\frac{\pi k_p}{D} \right)^{\frac{1}{2}}$$

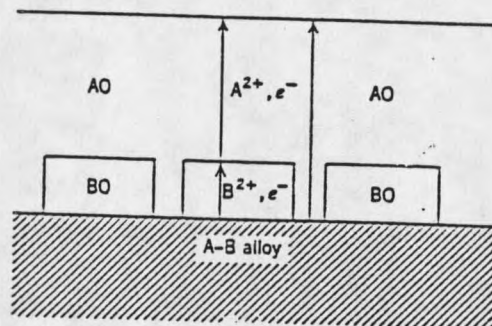
where V is the molar volume of the alloy, z_B is the valence of the B atoms, M_O is the atomic weight of oxygen, D is the diffusion coefficient of B in the alloy, and k_p is the parabolic rate constant for the exclusive formation of the B oxide.

The same type of assumptions can be made for composite scales that are practically insoluble in each other. For the case of formation of scales with complex oxides, diffusion rates are often appreciably smaller than in single oxides. The protective scales on high-temperature oxidation-resistant alloys often consist of complex oxides (double oxides, spinels etc.) [16].



(A)

(B)



(C)

Diffusion Processes During Oxidation of A-B Alloys

- (A) Exclusive Formation of A Oxide
- (B) Selective Oxidation of B Oxide
- (C) Simultaneous Formation of A-Oxide (AO) and B Oxide (BO)

B Oxide Grows According to the Displacement Reaction

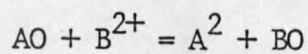


Figure 2. Wagner Schematics for Oxidation of Metal Alloys

CHAPTER 4

EXPERIMENTAL METHOD

Auger Electron Spectroscopy

Auger-electron spectroscopy (AES) is based on the Auger radiationless process [21]. The energetics of the Auger process, is shown in Figure 3. This process involves an electron excitation, which leaves a hole in a core level of an atom. This preliminary excitation process can be stimulated by absorption of energy from a primary electron. After the excitation process, the core hole is filled by an Auger recombination process. In the Auger recombination processes the core hole is filled by an electron occupying a higher energy level, that is, either a shallower core electron or a valence electron. The energy lost by this electron is transferred to another electron. This last electron may receive enough energy to leave the system, thus becoming an Auger electron.

The whole process, excitation plus Auger recombination, is usually labeled using the conventional spectroscopic notations for the initial states of the three electrons involved [22]. If the excitation involves a hole in a $1s$ state and this hole is filled by an electron in the $2s$ state that transfers its energy to another electron in the $2s$ state, then the entire process is labeled KL_1L_2 . In this notation the

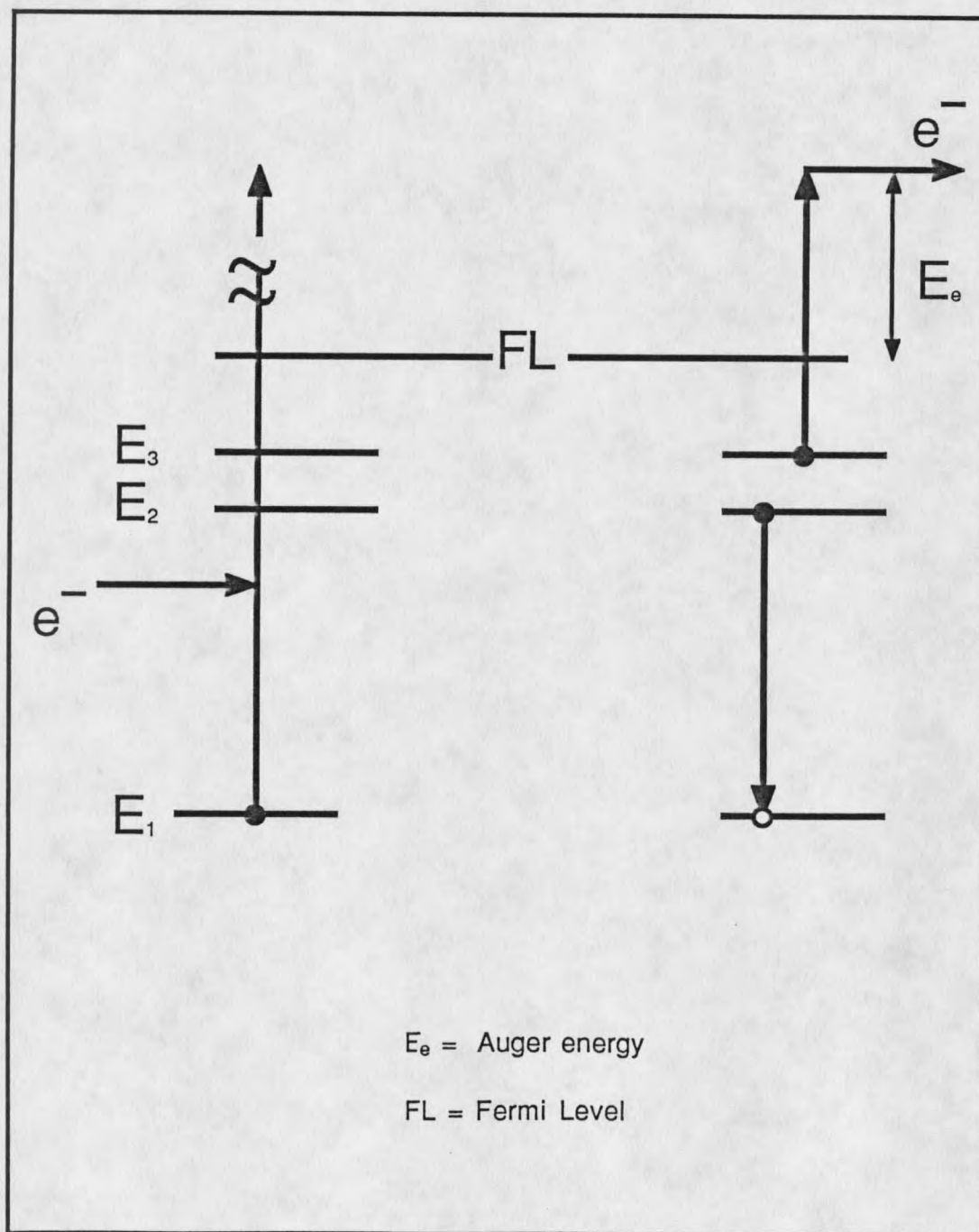


Figure 3. Energetics of the Auger Process

valence states are denoted by the letter v. Thus the final energy of the Auger electrons is linked to the energies of the three electron states. Therefore the emission of Auger electrons at a given energy reveals the presence of certain energy levels in the system. Since those levels are characteristic of a given element, it also reveals the presence of that element in the system. This provides for the analytical capability of AES. The exact link between the kinetic energy of the emitted Auger electrons and the core-level energies is complicated by factors such as electronic relaxation on formation of a core hole and final-state multiplet interactions. Nevertheless, the uncorrected binding energies of the three electrons are the most important factor in determining the Auger-electron kinetic energy.

Neglecting all factors except the uncorrected binding energies, and calling these energies E_1 , E_2 and E_3^* , for the first excited electron, the electron that fills the core hole, and the Auger electron, respectively, the kinetic energy of the latter can be written as:

$$E_k = E_3^* + E_2 - E_1$$

This equation is derived by estimating the energy of the two-hole final states in two subsequent steps, one creating a hole in state 2 and the other creating a hole in state 3. The energies in this equation are measured from the zero of the kinetic-energy scale, that is, from the vacuum level. The asterisk in the binding energy term E_3^* means that this is not

the unperturbed binding energy but rather the binding energy in the presence of another core hole.

The Auger electrons [7] thus have unique energies for each atom and if the energy spectrum from about 0 to 2 keV is analyzed, the energies of the Auger electron peaks allow for the identification of the surface elements present, except hydrogen and helium. The reason that AES is a surface-sensitive technique lies in the intense inelastic scattering that occurs for electrons in this energy range. Only Auger electrons from the top few atomic layers of a solid survive to be ejected and measured.

An Auger electron spectroscopy system consists of an ultra-high vacuum test system, an electron gun for specimen excitation and an energy analyzer for detection of Auger electron peaks in the total secondary electron energy spectrum [21].

Experimental System

Ultra-High Vacuum Systems

A UHV system is required for AES for two reasons. First and foremost, the electrons emitted from a specimen should meet as few gas molecules on their way to the analyzer as possible so that they are not scattered [23]. More importantly the reduction of contamination on the surfaces under analysis by the residual gases in the vacuum establishes a necessary base pressure of about 1×10^{-9} torr (1 torr = 1 mm. Hg

pressure). Such a pressure falls into the regime of ultra-high vacuum (UHV). This greatly restricts the use of materials in AES. For the system used in the present AES study most materials used in fabrication are stainless steel with copper gaskets used as a sealing material between conflat flanges [7].

The system assembly including the two turbomolecular pumps, the electron gun, the ion gun and the vacuum chamber is shown in Figure 4. The vacuum chamber is divided into two sections, a main section and a differential section. The turbomolecular pumps differentially pump the ion gun as well as differentially pump a vacuum seal on the sample manipulator in the main chamber. Pumping speed is increased by using separate pumps on the two chambers. The two pumping systems each include a roughing pump and a turbomolecular pump. They reduce the main chamber and differential chamber to base pressures of about 1.5×10^{-9} and 1×10^{-9} torr, respectively, after bakeout. The bakeout involves increasing the system temperature to about 150°C for a few hours in order to remove most of the volatile contaminants.

Ion Gun

Argon ion bombardment is a method of producing a clean surface and can be used in conjunction with surface analysis to measure compositional information as a function of depth [24]. Depth profiling is a technique which involves simultaneous ion bombardment and analysis (AES analysis in

